Supporting Material: Feedback mechanism for microtubule length regulation by bistable stathmin gradients

Maria Zeitz, Jan Kierfeld

Physics Department, TU Dortmund University,
44221 Dortmund, Germany

November 27, 2014

The Supporting Material contains details of the simulation methods for the feedback system of polymerizing microtubules, localized Rac1 and cytosolic stathmin. We also present additional model equations and simulation results on the stathmin activation gradient. We show additional results on the interrupted feedback subsystem without Rac and constitutively active stathmin. For the full system with closed feedback, we present details of the theoretical bifurcation analysis. Finally, we present additional results on the robustness of our results with respect to changes in the catastrophe model and the system length.

1 Simulation methods

The model described in the main text is the basis for our one-dimensional stochastic simulation. We employ a stochastic simulation with equal time steps $\Delta t = 0.001$s, i.e., the simulation time is discretized into equidistant discrete times $t_n = n\Delta t$. We model the MTs as straight polymers with continuous length, and Rac and Stathmin distributions via discrete particles, which can be activated and deactivated according to the rates specified in the main text. Stathmin particles can diffuse freely within the simulation box, whereas Rac particles are localized at the cell-edge region.

In Table 2 in the main text we present our choice of parameters to perform simulations. We assume a tubulin concentration $[T_0] = 19.4\mu$M, and we assign a volume $0.86\mu m^3$ to our simulation box, which is equivalent to a total number of $N_T = 10000$ tubulin dimers in the simulation box. We choose a simulation box of length $L = 10\mu$m with a cell-edge region of size $\delta = 20$nm, where Rac can be activated by MTs.

1.1 Microtubule simulation

In order to simulate one single MT in a box, we use the following approximations:

1) The MT is rigid and grows and shrinks in only one direction, along the x-axis. The MT tip position is described by a continuous variable x_{MT}.

2) The one-dimensional box has fixed rigid walls at $x = 0, L$. At $x_{\mathrm{MT}} = L$ (the cell edge), a growing MT experiences an immediate catastrophe event. For simplicity, we assume that at $x_{\mathrm{MT}} = 0$, a shrinking MT starts to grow again.

3) Tubulin is not simulated explicitly. The interaction with stathmin is implemented indirectly by a change of the growth velocity via the concentration $[T]$ of free tubulin following Eq. (6) in the main text. The total number $N_T = 10000$ of tubulin dimers is only needed to calculate values of stathmin/tubulin $s = S/[T_0] = N_S/N_T$ conveniently.

The MT is completely described by the position x_{MT} of the tip and its growth state (growing or shrinking). The switching of the MT state is described as a stochastic event with the time constant probabilities for catastrophe $p_c = \omega_c \Delta t$ and rescue $p_r = \omega_r \Delta t$ in each time step. Whereas the rescue rate ω_r is always independent of the MT tip position x_{MT}, the catastrophe rate $\omega_c(x_{\mathrm{MT}})$ becomes a function of x_{MT} in the presence of a stathmin concentration profile as further explained below. If the MT has grown in the last time step and a random number $c \in [0; 1]$ is smaller than p_c, then the MT shrinks in the current time step, and if $c > p_c$ the MT continues to grow (and vice versa). The new coordinate is

$$x_{\mathrm{MT},n+1} = x_{\mathrm{MT},n} + v_{+,n}\Delta t \quad \text{or} \quad x_{\mathrm{MT},n+1} = x_{\mathrm{MT},n} - v_{-}\Delta t \tag{S1}$$

for growing or shrinking respectively. At the boundary of the simulation box for positions $x_{\mathrm{MT}} > L$ a catastrophe is enforced, $p_c = 1$, and for $x_{\mathrm{MT}} < 0$, we enforce immediate rescue, $p_r = 1$. The growth velocity $v_{+,n}$ depends on the local concentration of free tubulin at $x_{\mathrm{MT},n}$ via Eq. (6) in the main text and, for tubulin-sequestering stathmin, on the local concentration of active stathmin via Eq. (14) in the main text.

In general, we perform simulations with m MTs, in a sufficiently big ensemble (in average 100 independent systems compose an ensemble). In order to minimize fluctuations, the observables are measured in the steady state and averaged over sufficiently large time intervals.

In order to measure the length distribution, i.e., the probability to find a MT of length x during the simulation, we divide the box into bins of the length ΔL and typically use $\Delta L = L/50$.

1.2 Rac simulation

The N_R Rac proteins are described as point-like objects which are all situated in the right boundary at $x = L$, which represents the cell edge. In each simulation time step Δt, each

Rac protein is deactivated with the constant probability $p_{\mathrm{off,R}} = k_{\mathrm{off,R}}\Delta t$. If a Rac protein is active, we draw a random number $c \in [0;1]$; if c is smaller than $p_{\mathrm{off,R}}$ it is deactivated in the following time step.

In order to activate Rac, a membrane contact of the MT is necessary. If one of the m MTs is at the cell edge region, each Rac protein is activated with a probability $p_{\mathrm{on,R}} = k_{\mathrm{on,R}}\Delta t$ in each time step Δt. If one MT is at the position $x_{\mathrm{MT}} \in [L-\delta; L]$ and a random number $c \in [0;1]$ is smaller than $p_{\mathrm{on,R}}$ the protein is activated in the next time step. Since the details of the Rac activation are not known, we include $\delta \ll L$ as a reaction distance.

1.3 Stathmin simulation

The N_S stathmin proteins are point-like objects which diffuse freely within the one-dimensional box $x \in [0, L]$. The probability density function for the distance Δx that a diffusing particle moves in a simulation time step Δt is a Gauss distribution

$$p(\Delta x, \Delta t) = \frac{1}{\sqrt{4\pi D \Delta t}} e^{-\frac{\Delta x^2}{4D\Delta t}}. \tag{S2}$$

The mean square distance a particle moves during the time step Δt is $\langle \Delta x^2 \rangle = 2D\Delta t$. We determine the new position of a stathmin protein (index j) as

$$x_{j,n+1} = x_{j,n} + d\sqrt{2D\Delta t}, \tag{S3}$$

where d denotes a random number drawn from a standard normal distribution. using a Box-Muller algorithm. The position $x_{j,n} \in [0; L]$ is limited to the box by reflecting boundary conditions.

We activate each stathmin protein regardless of its position within the cell with the probability $p_{\mathrm{on,S}} = k_{\mathrm{on,S}}\Delta t$ in each simulation time step Δt. This is implemented by comparison of $p_{\mathrm{on,S}}$ with a random number $c \in [0;1]$. The deactivation of a stathmin protein, on the other hand, only takes place if it is positioned in the interval $[L-\delta; L]$. Then, it is deactivated with the probability $p_{\mathrm{off,S}} = r_{\mathrm{on}} k_{\mathrm{off,S}}\Delta t$, with r_{on} being the fraction of active Rac proteins at this time step. Activation and deactivation are implemented by comparison of $p_{\mathrm{on,S}}$ and $p_{\mathrm{off,S}}$, respectively, with a random number $c \in [0;1]$.

We compare two mechanisms for the inhibition of MT growth by stathmin: (a) tubulin sequestering by stathmin resulting in reduced free tubulin concentrations, reduced MT growth velocities, and increased MT catastrophe rates and (b) a purely MT catastrophe-promoting activity of stathmin.

For both mechanisms, we measure the local concentration $S_{\mathrm{on}}(x)$ of active stathmin during the simulation, in order to simulate the local impact of stathmin on the growth velocity of a MT with tip position x. In order to define and measure the local concentration $S_{\mathrm{on}}(x)$ of active stathmin during the simulation, we divide the box into bins of the length

ΔL and count the active and inactive stathmin proteins. Because we choose ΔL much smaller than the stathmin gradient scale χ_S, see (S8) below, the total number of stathmin proteins is nearly constant in each bin. Typically, we choose $\Delta L = L/50$.

1.3.1 Tubulin-sequestering stathmin

For the tubulin-sequestering model of stathmin, we do not simulate the binding of tubulin dimers to stathmin explicitly but assume that the binding to stathmin is fast compared to the other processes. Therefore, we can determine the local concentration $t(s_{\mathrm{on}}(x))$ of free tubulin from the local concentration of active stathmin $s_{\mathrm{on}}(x) = S_{\mathrm{on}}(x)/[T_0]$ via the chemical equilibrium relation (14) for a fixed total tubulin concentration $[T_0]$ corresponding a number $N_T = [T_0]V$ of tubulin dimers in a volume V. Once we know the local concentration $[T](x) = [T_0]t(s_{\mathrm{on}}(x))$ of free tubulin, Eq. (6) in the main text determines the local growth velocity,

$$v_+ = v_+([T](x)) = v_+([T_0]t(s_{\mathrm{on}}(x))) \tag{S4}$$

(see Eq. (15) in the main text). This quasi-equilibrium relation allows us to determine the local MT growth velocity $v_+ = v_+(x)$ uniquely from the local concentration $S_{\mathrm{on}}(x)$ of active stathmin.

Because the catastrophe rate ω_c is determined by $v_+ = v_+(x)$ via relation (7) in the main text, a local growth velocity also gives rise to a local catastrophe rate $\omega_c = \omega_c(v_+(x))$ in the tubulin-sequestering model of stathmin.

1.3.2 Catastrophe-promoting stathmin

For the catastrophe-promoting model of stathmin, the local concentration $S_{\mathrm{on}}(x)$ of active stathmin does not affect the MT growth velocity v_+ but directly the catastrophe rate via the relation (16) in the main text. This gives rise to a local catastrophe rate $\omega_c = \omega_c(S_{\mathrm{on}}(x))$.

2 Gradient in stathmin activation

The interplay of stathmin diffusion and phosphorylation by active Rac at the cell edge establishes a spatial gradient of stathmin activation, for which we provide a detailed mathematical model here.

Stathmin proteins are either in an active dephosphorylated state with concentration profile $S_{\mathrm{on}}(x)$ or in an inactive phosphorylated state with concentration profile $S_{\mathrm{off}}(x)$ (with a total stathmin concentration $S_{\mathrm{tot}}(x) = S_{\mathrm{on}}(x) + S_{\mathrm{off}}(x)$). In both states, stathmin diffuses freely within the model box $x \in [0; L]$ with a constant diffusion coefficient D, which is equal for both states. Switching between active and inactive state is a stochastic process with rates $k_{\mathrm{on,S}}$ and $k_{\mathrm{off,S}}$.

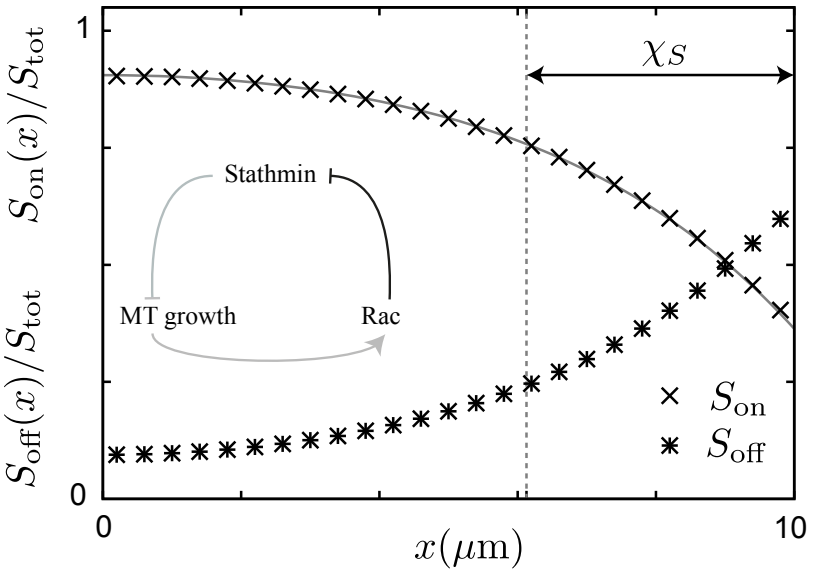

Figure S1: Spatial gradient of stathmin activation for constitutively active Rac. Data points show results from stochastic simulations, lines the analytical result (11) (for $r_{\mathrm{on}} = 1$). Parameters are as in Table 2 in the main text resulting in $\chi_S \simeq 3.87\,\mu$m. There are no fit parameters.

Moreover, active Rac deactivates stathmin at the cell edge $x = L$ as simple second order reaction with a rate proportional to r_{on}. The resulting chemical kinetics for the boundary value $S_{\mathrm{off}}(L)$ (strictly speaking the values in the cell-edge region $[L-\delta, L]$) including diffusion away from the cell edge can then be described by

$$\frac{\partial S_{\mathrm{off}}(L)}{\partial t} = -\frac{D}{\delta}\left.\frac{\partial S_{\mathrm{off}}}{\partial x}\right|_{x=L} + k_{\mathrm{off,S}} r_{\mathrm{on}} S_{\mathrm{on}}(L) - k_{\mathrm{on,S}} S_{\mathrm{off}}(L). \tag{S5}$$

We assume that the phosphatase responsible for stathmin activation is homogeneously distributed within the cytosol such that stathmin dephosphorylates everywhere within the box with the constant rate $k_{\mathrm{on,S}}$ (1) (which depends on the concentration of the homogeneously distributed stathmin phosphatase). The distribution of deactivated stathmin in the one-dimensional box is then described by the reaction-diffusion equation

$$\frac{\partial S_{\mathrm{off}}}{\partial t} = D\frac{\partial^2 S_{\mathrm{off}}}{\partial x^2} - k_{\mathrm{on,S}} S_{\mathrm{off}}. \tag{S6}$$

This equation is complemented by the boundary condition (S5) for $S_{\mathrm{off}}(L)$ and by a zero diffusive flux condition $D\,\partial S_{\mathrm{off}}/\partial x|_{x=0} = 0$ at $x = 0$. The distribution of active stathmin $S_{\mathrm{on}}(x)$ can be obtained analogously (using also $S_{\mathrm{tot}}(x) = S_{\mathrm{on}}(x) + S_{\mathrm{off}}(x)$).

Equations (S6) and (S5) describe the stathmin kinetics at the mean-field level; equation (S5) neglects temporal correlations between Rac and stathmin number fluctuations. by using the mean fraction $r_{\rm on}$ in the deactivation process.

In the steady state, the time derivatives in (S5) and (S6) vanish, and the total stathmin concentration $S_{\rm tot} = S_{\rm on}(x) + S_{\rm off}(x) = {\rm const}$ becomes homogeneous due to diffusion. The corresponding stationary solution of (S5) and (S6) for the stathmin activation gradient is

$$\frac{S_{\rm on}(x)}{S_{\rm tot}} = 1 - 2A\cosh(x/\chi_S), \tag{S7}$$

see Eq. (11) in the main text, with the characteristic decay length

$$\chi_S = \sqrt{D/k_{\rm on,S}}. \tag{S8}$$

The integration constant A depends on the degree of stathmin deactivation by Rac at the cell edge $x = L$ and, thus, on the fraction $r_{\rm on}$ of activated Rac. For a fixed level $r_{\rm on}$ of Rac activation, we find

$$A = \frac{1}{2}\frac{r_{\rm on}k_{\rm off,S}}{(D/\delta\chi_S)\sinh(L/\chi_S) + (r_{\rm on}k_{\rm off,S} + k_{\rm on,S})\cosh(L/\chi_S)}, \tag{S9}$$

see also Eq. (12) in the main text.

We can compare the analytical result (S7) for the concentration profile of active stathmin at a fixed fraction $r_{\rm on}$ of active Rac in Eq. (S9) with stochastic simulation results for a fixed level $r_{\rm on}$ of Rac activation (i.e., keeping $N_R r_{\rm on}$ of N_R Rac proteins in the simulation permanently in the activated state). In Fig. S1, we show this comparison for a subsystem with constitutively active Rac corresponding to $r_{\rm on} = 1$ in Eq. (S9) and see very good agreement without any adjustable fit parameters.

3 Interrupted feedback for constitutively active stathmin in the absence of Rac

In this section, we present additional results on MT length distributions for a subsystem without Rac, i.e., with constitutively active stathmin.

Without Rac, the constitutively active stathmin is homogeneously distributed, $S_{\rm tot} = S_{\rm on} = {\rm const}$. Therefore, also the length parameter λ is constant, see Eq. (4) in the main text, and the MT mean length is given by Eq. (5) in the main text.

Fig. S2 shows results for the mean MT length $\langle x_{\rm MT}\rangle$ as a function of stathmin/tubulin $s = S_{\rm tot}/[T_0]$, and insets show the corresponding MT length distribution at three different stathmin/tubulin s. Fig. S2 (A) shows results for tubulin-sequestering stathmin, Fig. S2 (B) for catastrophe-promoting stathmin. We find good agreement between the analytical

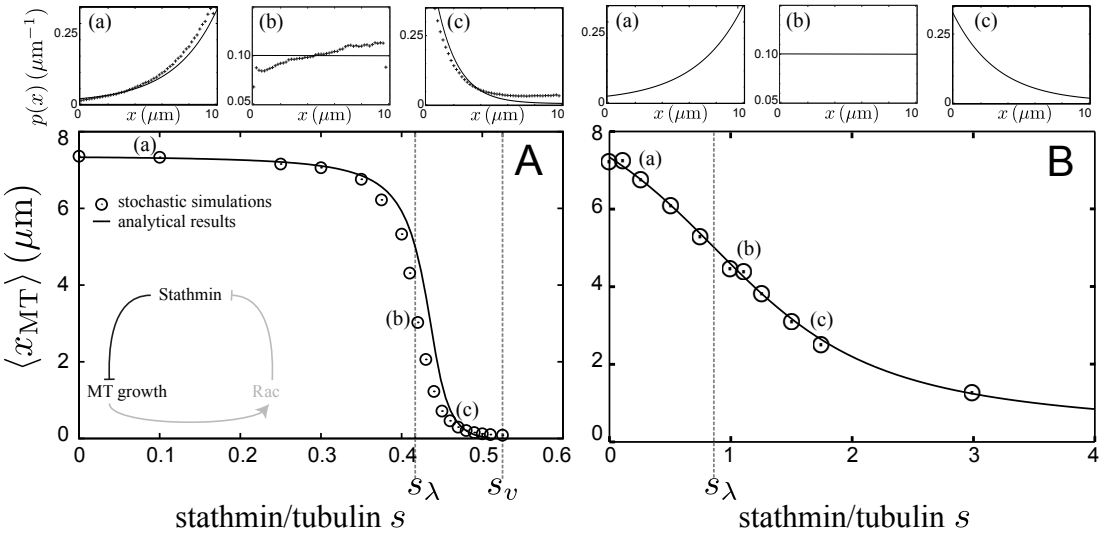

Figure S2: Stochastic simulation data and analytical master equations results for the system without Rac ($r_{\rm on} = 0$) and constitutively active stathmin for tubulin-sequestering stathmin (A) and catastrophe-promoting stathmin (B). We show results for the mean MT length $\langle x_{\rm MT}\rangle$ in the steady state as a function of stathmin/tubulin $s = S_{\rm tot}/[T_0]$. The black curves correspond to the analytical result Eq. (5) in the main text, black symbols to stochastic simulation results. The critical concentrations s_λ and s_v are indicated. The insets (a), (b), (c) show MT length distributions for three particular values of s, which are also indicated in the main plot, with (a) $s < s_\lambda$, (b) $s = s_\lambda$ and (c) $s > s_\lambda$; curves are the analytical result Eq. (3) in the main text, symbols are stochastic simulation results.

result (5) from the main text (lines) and stochastic simulation results (data points) both for tubulin-sequestering and catastrophe-promoting stathmin.

The two critical concentrations s_λ and s_v control the mean length $\langle x_{\rm MT}\rangle$, as we see in Fig. S2. For $s = s_\lambda$, we have $\langle x_{\rm MT}\rangle = L/2$, for $s \geq s_v$, we have $\langle x_{\rm MT}\rangle = 0$ according to their definition (see main text).

For tubulin-sequestering stathmin and simulation parameters as given in Table 2 in the main text corresponding to $[T_0] = 19.4\mu$M or a total number of $N_T = 10000$ tubulin molecules in the simulation box, the critical concentrations of stathmin molecules (normalized by the total tubulin concentration $[T_0]$) are

$$s_\lambda = \frac{S_\lambda}{[T_0]} = \frac{N_{S,\lambda}}{N_T} = 0.419 \quad \text{and} \quad s_v = \frac{S_v}{[T_0]} = \frac{N_{S,v}}{N_T} = 0.528. \tag{S10}$$

The values s_λ and s_v are only weakly $[T_0]$-dependent; for $[T_0]$ in the range $[T_0] = 10-20\mu$M,

we find $s_\lambda = 0.34 - 0.42$ and $s_v = 0.51 - 0.53$.

For catastrophe-promoting stathmin, the MT growth velocity is not affected by stathmin, which formally results in an infinite S_v. A critical concentration S_λ can still be defined in the same way, and we find $S_\lambda = (v_+\omega_r - v_-\omega_c(0))/k_c v_-$ from Eqs. (4) and (16) in the main text. The MT growth velocity v_+ is linearly increasing with $[T] = [T_0]$, see Eq. (6) in the main text, and $\omega_c(0)$ correspondingly decreasing according to Eq. (7) in the main text. For high tubulin concentrations, s_λ approaches the $[T_0]$-independent limit $s_\lambda \approx \kappa_{\rm on} d\omega_r/v_-k_c = 0.91$, which is significantly above the typical values close to 0.5 for tubulin-sequestering stathmin. For the simulation parameters as given in Table 2 in the main text corresponding to $[T_0] = 19.4\mu$M or a total number of $N_T = 10000$ tubulin molecules in the simulation box, the critical concentration of stathmin molecules (normalized by the total tubulin concentration $[T_0]$) is

$$s_\lambda = \frac{S_\lambda}{[T_0]} = \frac{N_{S,\lambda}}{N_T} = 0.866. \tag{S11}$$

The value s_λ is only weakly $[T_0]$-dependent, for $[T_0]$ in the range $[T_0] = 10 - 20\mu$M, we find $s_\lambda = 0.79 - 0.87$.

The stochastic simulation results for the MT length distribution also agree with the analytical result (3) in the main text. At the critical stathmin concentration $s = s_\lambda$, the condition $\lambda^{-1} = 0$ results in a flat MT length distribution, as confirmed in inset (b) in Fig. S2. For $s > s_\lambda$, we find the length distribution of the MT to be a negative exponential (see inset (c) in Fig. S2). For $s < s_\lambda$, we find the length distribution of the MT to be a positive exponential (see inset (a) in Fig. S2). For a system which contains constitutively active stathmin and no Rac, the growth velocity v_+ is independent of the position (not taking into account the small diffusion-induced fluctuations of the local stathmin concentration). Therefore, we always expect an exponential MT length distribution according to Eq. (3) in the main text. In particular, we do not expect bimodal MT length distributions in the absence of Rac, as confirmed by the stochastic simulation in the insets in Fig. S2.

4 Bifurcation analysis for closed feedback

In the bifurcation analysis we consider the stationary system state for a closed feedback loop.

A given fraction $r_{\rm on}$ of activated Rac then determines the MT contact probability $p_{\rm MT} = m\int_{L-\delta}^{L} p_+(x,t)$ (see Eq. (9) in the main text) via (i) a stationary gradient in stathmin activation (a decreasing profile $S_{\rm on}(x)$), (ii) a resulting MT growth velocity gradient (an increasing growth velocity $v_x(x)$) established by tubulin sequestering, and (iii) the resulting stationary MT length distribution and, in particular, the probability $p_+(x)$ to find a particular MT in the growing state. These three dependencies can be described analytically and the resulting equations can be easily evaluated numerically:

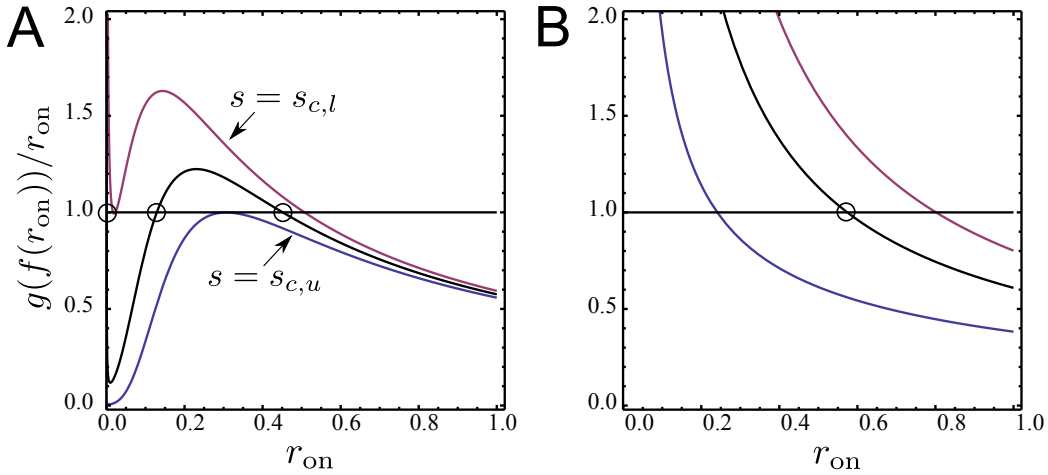

Figure S3: Function $g(f(r_{\rm on}))/r_{\rm on}$ for $m = 1$ and three different values of stathmin/tubulin $s = S_{\rm tot}/[T_0]$ for (A) tubulin-sequestering stathmin and (B) catastrophe-promoting stathmin. For tubulin-sequestering stathmin (A), the lines are for $s = s_{c,l} = 0.446$ (blue), $s = s_{c,u} = 0.459$ (red), and $s = 0.453$ (black). For $s_{c,l} < s < s_{c,u}$ (black line $s = 0.453$) there exist three fixed points (circles). The middle fixed point is unstable. For catastrophe-promoting stathmin (B) the lines are for $s = 0.1$ (blue), $s = 1.7$ (red), and $s = 1.1$ (black). There is always a single fixed point.

(i) The stationary gradient in stathmin activation can be calculated by Eq. (11) in the main text, where $r_{\rm on}$ enters the gradient amplitude A, which is given by Eq. (12) in the main text. This allows us to calculate the stathmin activation profile $S_{\rm on}(x)/S_{\rm tot}$ for any fixed level $r_{\rm on}$ of activated Rac. For constitutively active Rac, $r_{\rm on} = 1$, the result is shown and tested versus stochastic simulations in Fig. S1.

(ii) From the stathmin activation gradient $S_{\rm on}(x)/S_{\rm tot}$ we obtain $s_{\rm on} = S_{\rm on}(x)/[T_0] = s(S_{\rm on}(x)/S_{\rm tot})$ with the total stathmin/tubulin $s = S_{\rm tot}/[T_0]$. For tubulin-sequestering stathmin, this is used to determine the spatially dependent tubulin concentration $[T](x) = [T_0]t(s_{\rm on}(x))$ through Eq. (14) in the main text. This free tubulin concentration profile can be used to calculate the MT growth velocity profile $v_+ = v_+([T_0]t(s_{\rm on}(x)))$ according to Eq. (15) in the main text.

(iii) For tubulin-sequestering stathmin, the position-dependent growth velocity $v_+(x)$ also gives rise to a position-dependent catastrophe rate $\omega_c = \omega_c(v_+(x))$ (see Eq. (7) in the main text). For catastrophe-promoting stathmin, the stathmin activation gradient directly gives rise to position-dependent catastrophe rate $\omega_c = \omega_c(S_{\rm on}(x))$ via relation

(16) in the main text. Finally, we obtain a position dependent MT growth parameter $\lambda(x) = v_+(x)v_-/(v_+(x)\omega_r - v_-\omega_c(x))$ for both models of stathmin action (see Eq. (4) in the main text). This allows us to calculate the relevant MT length distribution $p_+(x)$ according to Eq. (17) from the main text.

This scheme allows us to calculate $p_+(x)$ and, thus, p_{MT} for any fixed level $r_{\rm on}$, i.e., to implement a function $p_{\rm MT} = f(r_{\rm on})$. Vice versa, for a closed feedback, the contact probability also determines the Rac activation level $r_{\rm on}$ via (10) in the stationary state, which specifies a second function $r_{\rm on} = g(p_{\rm MT})$. At the stationary state for closed feedback, the fixed point condition $r_{\rm on} = g(f(r_{\rm on}))$ has to hold, which selects possible fixed point values $r^*_{\rm on}$ for the Rac activation level $r_{\rm on}$. If

$$\left.\frac{dg(f(r))}{dr}\right|_{r=r^*_{\rm on}} < 1 \tag{S12}$$

the fixed point is stable, otherwise it is unstable. For a stable fixed point, an increase $\delta r_{\rm on}$ in $r_{\rm on}$ by perturbation gives rise to a down-regulation of $r_{\rm on}$ because the corresponding increase $\delta p_{\rm MT}$ is not sufficient to maintain the increased level $r_{\rm on} + \delta r_{\rm on}$.

Analyzing the function $g(f(r_{\rm on}))$ for tubulin-sequestering stathmin, we find two saddle-node bifurcations typical for a bistable switch. For stathmin/tubulin $s = S_{\rm tot}/[T_0]$ between a lower critical value $s_{c,l}$ ($s_{c,l} = 0.446$ for $m = 1$ increasing to $s_{c,l} = 0.453$ for $m = 10$) and an upper critical value $s_{c,u}$ ($s_{c,u} = 0.459$ for $m = 1$ increasing to $s_{c,u} = 0.492$ for $m = 10$ and approaching $s_{c,u} \approx s_v = 0.528$ for large m) there exist three fixed points, the middle one of which is unstable (see Fig. S3 A).

This bifurcation behavior represents a bistable switch with stathmin/tubulin s as control parameter as can be clearly seen from Fig. S4. In the left Fig. S4, the Rac activation fixed points $r^*_{\rm on}$ are shown as a function of s. In the right Fig. S4, the corresponding average MT length $\langle x_{\rm MT}\rangle$ is shown.

For catastrophe-promoting stathmin we always find a *single* fixed point and no sign of a bifurcation for all stathmin/tubulin $s = S_{\rm tot}/[T_0]$ values (see Fig. S3 B).

5 Robustness of results

In this section, we address the robustness of our results with respect to changes in the catastrophe model and the system length.

5.1 Robustness with respect to the catastrophe model

The catastrophe model described by Eq. (7) in the main text and used throughout the manuscript is based on the experimental results by Janson *et al.* (2) and, in this sense, of phenomenological nature. Other catastrophe models have been formulated in the literature.

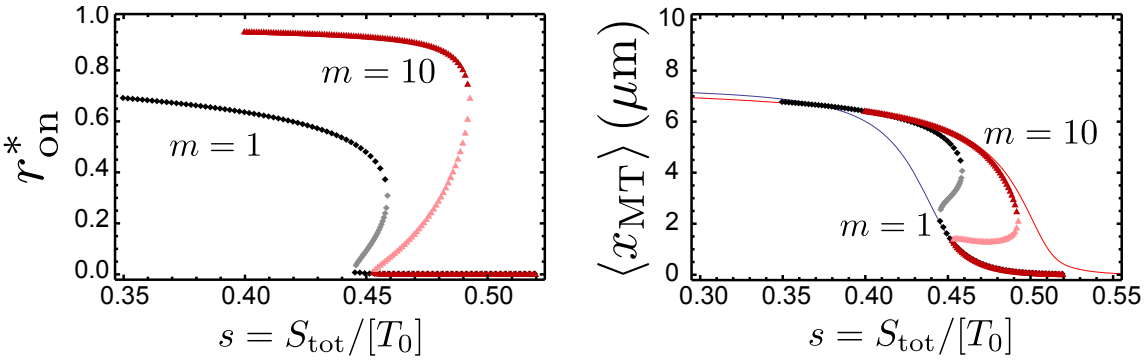

Figure S4: Left: Rac activation fixed points $r^*_{\rm on}$ for tubulin-sequestering stathmin as a function of stathmin/tubulin $s = S_{\rm tot}/[T_0]$ for $m = 1$ (black data points) and $m = 10$ (red data points). For $s_{c,l} < s < s_{c,u}$ there exist three fixed points. The middle fixed point are unstable (light red and light black data points). Right: Corresponding average MT length $\langle x_{\rm MT}\rangle$ for the fixed point values $r^*_{\rm on}$ as a function of s. Lines show the average MT length $\langle x_{\rm MT}\rangle$ for a system without Rac and constitutively active stathmin ($r_{\rm on} = 0$, blue line) and for constitutively active Rac ($r_{\rm on} = 1$, red line).

Because there is no strict consensus on a particular catastrophe model, it is important that results are robust with respect to a change of the catastrophe model.

Another frequently used catastrophe model due to Flyvbjerg *et al.* is based on an analytical calculation of the first passage rate to a state with vanishing GTP-cap for a model for cooperative hydrolysis of GTP-tubulin (3). In a cooperative model, hydrolysis proceeds by a combination of both random and vectorial mechanisms (4). In Ref. (3), the catastrophe rate has been calculated as implicit function of the growth velocity v_+ and two hydrolysis parameters v_h (characterizing the vectorial part) and r (characterizing the random part). The exact dimensionless catastrophe rate $\alpha \equiv \omega_c D^{-1/3} r^{-2/3}$ is given by the smallest solution of

$$Ai'(\gamma^2 - \alpha) = -\gamma Ai(\gamma^2 - \alpha) \tag{S13}$$

with $\gamma \equiv v D^{-2/3} r^{-1/3}/2$, where $v \equiv v_+ - v_h$ and $D \equiv (v_+ + v_h)d/2$ [$Ai'(x) \equiv dAi(x)/dx$]. Here Ai denotes the first Airy function. We use a numerical implementation of this analytical result in simulations and mean-field calculations: We solve Eq. (S13) numerically to calculate the function $\alpha = \omega_c D^{-1/3} r^{-2/3}$ as a function of γ. From this numerical solution we obtain the catastrophe rate as function of the MT growth velocity, $\omega_c = \omega_c(v_+)$. The hydrolysis parameters $v_h \simeq 4.2 \times 10^{-9}$ m/s and $r \simeq 3.7 \times 10^6\,{\rm m}^{-1}{\rm s}^{-1}$ (3) are fixed during the simulation.

Results for this alternative catastrophe model by Flyvbjerg *et al.* are shown in Fig.

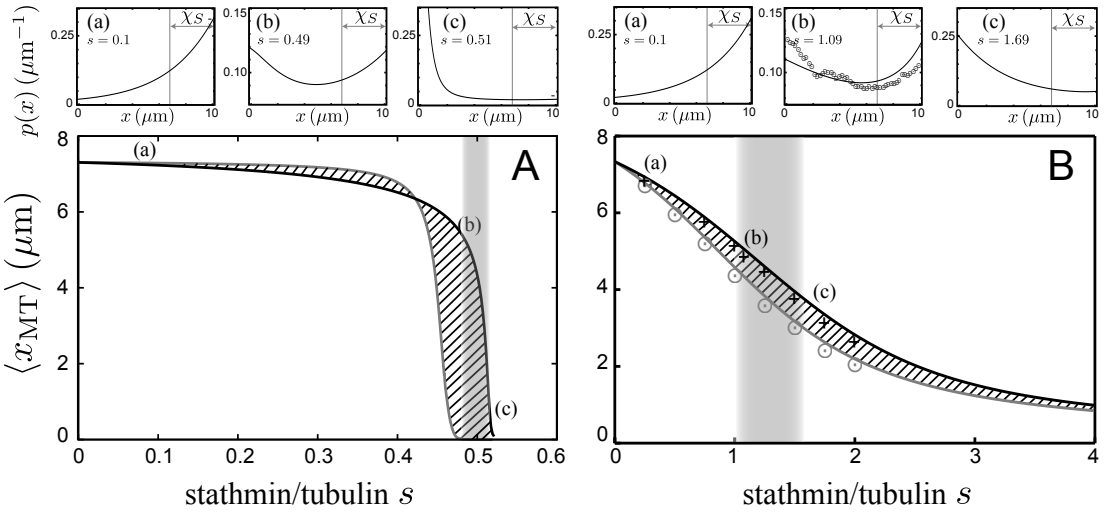

Figure S5: Results for the alternative Flyvbjerg catastrophe model analogously to Fig. 3 in the main text. Stochastic simulation data (data points) and analytical master equation results (solid lines) for the mean MT length $\langle x_{\mathrm{MT}} \rangle$ as a function of stathmin/tubulin $s = S_{\mathrm{tot}}/[T_0]$. We compare the system with constitutively active Rac ($r_{\mathrm{on}} = 1$, black lines and crosses) in comparison to the system without Rac ($r_{\mathrm{on}} = 0$, gray lines and circles) both for tubulin-sequestering stathmin (A) and catastrophe-promoting stathmin (B). The hatched area indicates the possible MT length gain by Rac regulation. The gray shaded area indicates the region, in which MTs exhibit bimodal length distributions for constitutively active Rac. The insets (a), (b), (c) show the corresponding MT length distributions for three particular values of s with (a) $s < s_\lambda$, (b) $s = s_\lambda$ and (c) $s > s_\lambda$.

S5. Analogously to Fig. 3 in the main text, we show both results for tubulin-sequestering stathmin (Fig. S5 A) and catastrophe-promoting stathmin (Fig. S5 B). We obtain the same main features using the alternative catastrophe model: We find a switchlike dependence of MT length on the overall stathmin/tubulin both for tubulin-sequestering and catastrophe-promoting stathmin. We obtain bimodal MT length distributions both for tubulin-sequestering and catastrophe-promoting stathmin. We find bistability for tubulin-sequestering stathmin (see Fig. S6), whereas there is no bistability for catastrophe-promoting stathmin.

5.2 Robustness with respect to the system length

Cells have different lengths. Therefore we also investigated the robustness of our results with respect to changes in the system length L. In the main text we used $L = 10\,\mu$m,

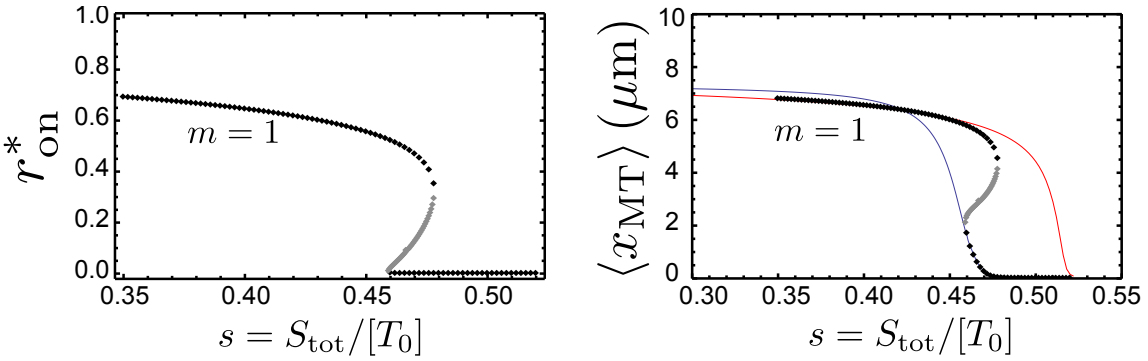

Figure S6: As in Fig. S4 but for the Flyvbjerg catastrophe mode. Left: Rac activation fixed points $r^*_{\rm on}$ for tubulin-sequestering stathmin as a function of stathmin/tubulin $s = S_{\rm tot}/[T_0]$ for $m = 1$. For $s_{c,l} < s < s_{c,u}$ there exist three fixed points. The middle fixed point are unstable (light black data points). Right: Corresponding average MT length $\langle x_{\rm MT}\rangle$ for the fixed point values $r^*_{\rm on}$ as a function of s. Lines show the average MT length $\langle x_{\rm MT}\rangle$ for a system without Rac and constitutively active stathmin ($r_{\rm on} = 0$, blue line) and for constitutively active Rac ($r_{\rm on} = 1$, red line).

here we present additional simulation results for a longer system $L = 20\,\mu$m in Fig. S7. It is important to notice that one *fixed* length scale within the feedback loop is set by the characteristic scale $\chi_S = \sqrt{D/k_{\rm on,S}}$ (see Eq. (S8)) of the stathmin activation gradient. For parameters as in Table 2 in the main text, we have $\chi_S \simeq 3.87\,\mu$m. The length scale χ_S is the typical size of the cell-edge region $L - \chi_S < x < L$ in which stathmin is deactivated. The stathmin activation profile becomes very flat in the remaining region $0 < x < L - \chi_S$, which increases in size if the system size L is increased.

Qualitatively, we find the same behavior for a longer system $L = 20\,\mu$m as for the shorter system $L = 10\,\mu$m with a switchlike dependence of MT length on the overall stathmin/tubulin, a bimodal MT length distributions both for tubulin-sequestering and catastrophe-promoting stathmin and bistability only for tubulin-sequestering stathmin. As a result of the more shallow gradient in large parts of the cell, however, the switching behavior of the MT length as a function of the total stathmin level becomes steeper, see Fig. S7 for tubulin-sequestering stathmin. Accordingly, for tubulin-sequestering stathmin, the windows of stathmin concentrations, where we find bimodal MT length distributions and where we find bistability, are narrower for longer cells.

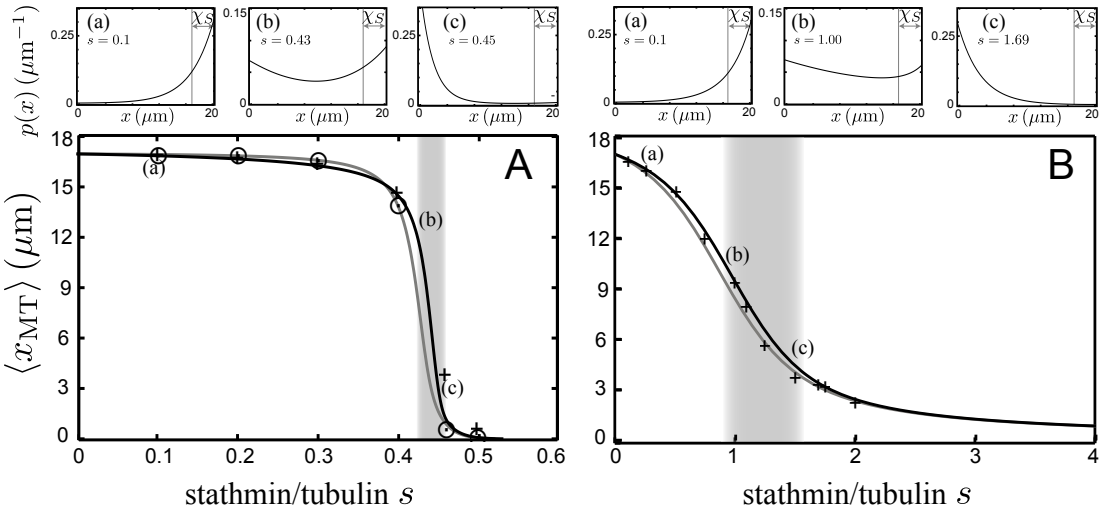

Figure S7: Results for a larger system of length $L = 20\,\mu$m, analogously to Fig. 3 in the main text, which is for $L = 10\,\mu$m. Stochastic simulation data (data points) and analytical master equation results (solid lines) for the mean MT length $\langle x_{\mathrm{MT}} \rangle$ as a function of stathmin/tubulin $s = S_{\mathrm{tot}}/[T_0]$. We compare the system with constitutively active Rac ($r_{\mathrm{on}} = 1$, black lines and crosses) in comparison to the system without Rac ($r_{\mathrm{on}} = 0$, gray lines and circles) both for tubulin-sequestering stathmin (A) and catastrophe-promoting stathmin (B). The gray shaded area indicates the region, in which MTs exhibit bimodal length distributions for constitutively active Rac. The insets (a), (b), (c) show the corresponding MT length distributions for three particular values of s with (a) $s < s_\lambda$, (b) $s = s_\lambda$ and (c) $s > s_\lambda$.

Supporting References

1. Brown, G. C., and B. N. Kholodenko. 1999. Spatial gradients of cellular phosphoproteins. *FEBS Lett.* 457:452–4.

2. Janson, M. E., M. E. de Dood, and M. Dogterom. 2003. Dynamic instability of microtubules is regulated by force. *J. Cell Biol.* 161:1029–34.

3. Flyvbjerg, H., T. E. Holy, and S. Leibler. 1996. Microtubule dynamics: Caps, catastrophes, and coupled hydrolysis. *Phys. Rev. E* 54:5538–5560.

4. Li, X., J. Kierfeld, and R. Lipowsky. 2009. Actin Polymerization and Depolymerization Coupled to Cooperative Hydrolysis. *Phys. Rev. Lett.* 103:048102.